Auger recombination and biexcitons in Cu_2O: A case for dark excitonic matter

J. I. Jang* and J. P. Wolfe†

Physics Department and Fredrick Seitz Materials Research Laboratory, University of Illinois at Urbana-Champaign, 1110 West Green Street, Urbana, Illinois 61801, USA

(Received 7 April 2006; published 24 July 2006)

The lifetime of excitons in Cu_2O decreases significantly at high gas densities. This effect has been attributed to an Auger recombination process between two excitons, resulting in a loss rate given by $\tau^{-1}=An$, where A is the Auger constant and n is the exciton gas density. Previous time- and space-resolved photoluminescence measurements, however, yielded an Auger constant that is orders of magnitude larger than theoretical calculations. In addition, the experimental Auger constant varied inversely with temperature, in contrast to the linear-T dependence predicted for direct Auger recombination of two free excitons. To resolve these discrepancies, we propose that excitons form biexcitons that rapidly decay by the Auger process. In this case, the lifetime of excitons is limited by exciton-exciton "capture" which occurs more frequently at low temperature. The instantaneous decay rate of excitons due to the capture process is given by $2\bar{C}n$ where $\bar{C}$ is a capture coefficient averaged over orthoexcitons and paraexcitons. Analysis of our photoluminescence data between 2 and 212 K is consistent with a paraexciton capture coefficient that depends inversely with gas temperature. Detailed analysis of the exciton transients following short-pulse excitation yields a biexciton binding energy ϕ roughly in the range 8–15 meV and a biexciton Auger rate $\tau_A^{-1}=0.5T$ ns^{-1} K^{-1}, where T is the gas temperature. Due to their short lifetimes, the density of biexcitons is predicted to be considerably lower than the density of excitons, and it is likely that the ground state of a biexciton is optically inactive. Consequently, it is not surprising that photoluminescence of biexcitons has not been observed in this crystal. The existence of such "dark matter" would explain the long-standing difficulties in achieving Bose-Einstein condensation of excitons in this system.

DOI: 10.1103/PhysRevB.74.045211 PACS number(s): 71.35.Cc, 71.35.Gg, 73.20.Mf

I. INTRODUCTION

Excitons in crystals of cuprous oxide (Cu_2O) are quite unique for several reasons: (i) spherical conduction and valence bands with relatively large effective masses produce an exciton with small Bohr radius (7 Å) and large binding energy (153 meV); (ii) the lowest conduction band and highest valence band in this direct-gap semiconductor have positive parity, causing long radiative lifetimes of excitons; (iii) excitons in high purity natural-growth crystals display phonon-limited mean free paths, exceeding 30 μm at 2 K; (iv) the 1s ground configuration of the exciton splits into ortho ($J=1$) and para ($J=0$) states that have clear photoluminescence signatures. The small Bohr radii of the excitons imply that their dissociation into an electron-hole plasma would require densities beyond 10^{20} cm^{-3}. In addition, neither excitonic molecules nor electron-hole liquid have been observed in this semiconductor using spectroscopic methods. Consequently, over a wide range of temperatures and densities, the excitons are believed to behave as an ideal gas of classical particles.[1]

Considering these properties, excitons in high-purity Cu_2O crystals would seem to be an excellent candidate for Bose-Einstein condensation (BEC).[1–8] The predicted critical density is about 10^{17} cm^{-3} at $T=2$ K, which should be readily achievable for excitons with microsecond lifetimes. Unfortunately, BEC has proven to be an elusive goal due to a strong recombination process that becomes effective at gas densities above about 10^{14} cm^{-3}. This undesirable decay mechanism has been characterized in terms of an exciton Auger effect.[9–15] Basically, when two excitons collide, one recombines and contributes its band-gap energy towards the kinetic energies of the remaining electron and hole. The result is the loss of an exciton accompanied by a heating of the remaining exciton gas. The theoretical basis for an exciton Auger process remains uncertain.[15] It is clear, however, that understanding and possibly controlling the density-dependent exciton lifetimes is essential to producing high densities of thermalized excitons in Cu_2O.

Figure 1(a) shows the primary supporting evidence for an Auger process. Time-resolved photoluminescence experiments measure the decay of exciton number $N(t)$ following short optical pulses. At the highest excitation power, the initial decay rate is nearly 50 times the final decay rate. From these data and separate measurements of the gas volume, it is possible to define and determine an exciton Auger constant A, given by the rate equation

$$\frac{dn}{dt}=-\frac{n}{\tau}-An^2, \tag{1}$$

where n is the exciton gas density and τ is the impurity-limited lifetime of the excitons. First experiments of this type by Warren *et al.*[11] obtained a value $A_{\text{expt}}\simeq 10^{-16}$ cm^3/ns at a temperature of 70 K. On the theoretical side, Kavoulakis and Baym (KB) (Ref. 16) considered several Auger decay processes and proposed a dominant mechanism involving the emission of an optical phonon. With a corrected deformation potential,[16] their theory for phonon-assisted Auger recombination of two excitons in Cu_2O predicts a value $A_{\text{phonon}}\simeq 3\times 10^{-22}$ cm^3/ns at 70 K, which is actually smaller than the direct (no-phonon) Auger constant $A_{\text{direct}}\simeq 2\times 10^{-21}$ cm^3/ns. Both theoretical predictions are orders of magnitude smaller

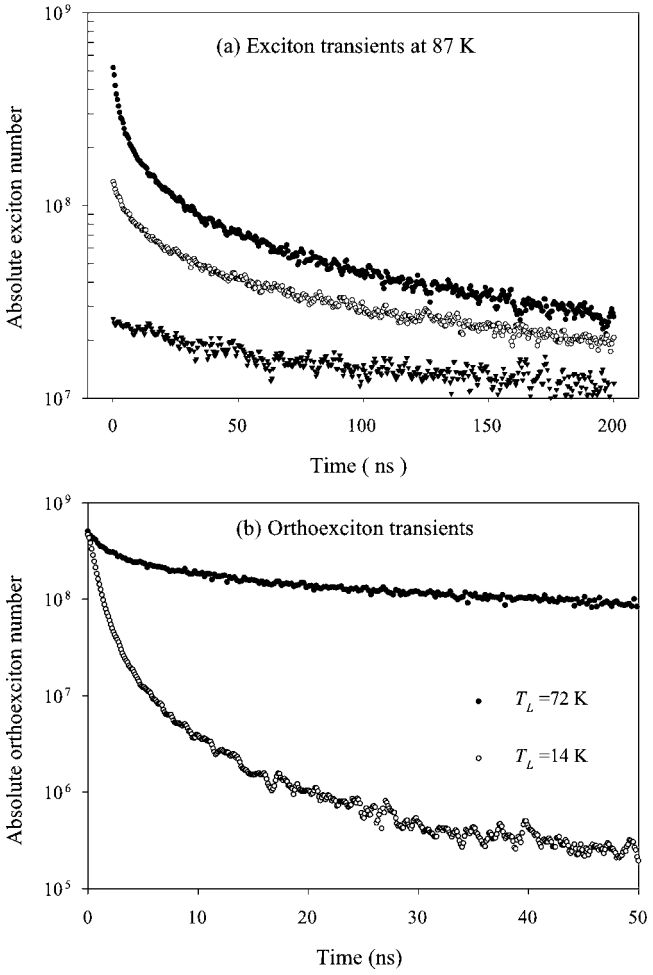

FIG. 1. (a) Photoluminescence transients recorded at the center of an exciton cloud following short optical pulses. Orthoexciton luminescence at 87 K is collected for three excitation powers, varying by a factor of about 20 and showing a density dependent decay rate. At this relatively high temperature, the population of ortho and para states are determined by Boltzmann statistics, so the data represent the decay of total exciton numbers. (b) Spectrally and spatially integrated orthoexciton transients showing two different regimes (i) high T_L (dots) and (ii) low T_L (circles). Calibration of the absolute number of excitons in the cloud is described later in this paper.

than measured in the experiments of Warren *et al.* and others.[10,12,14] Moreover, the theory for both processes predicts a linear increase in rate with increasing temperature,[17] whereas recent data[15] indicate an inverse-T dependence. These huge discrepancies between theory and experiment have led us to consider a possible mechanism for increasing the effectiveness of Auger decay: the formation of biexcitons (two electrons and two holes).[18]

Specifically we examine the possibility that two excitons bind into a biexciton that rapidly decays by the Auger process. As with the exciton Auger process, Auger decay of a biexciton produces a hot e-h pair with the energy gained from nonradiative recombination of the other e-h pair. Although biexcitons have not been directly observed in Cu_2O, the ground state of a biexciton (Γ_1^+) is not expected to be visible by either direct or phonon-assisted photoluminescence (or absorption) in this forbidden-gap material.[19] Thus the lack of spectroscopic evidence for biexcitons[20] in Cu_2O does not disprove their existence. The formation of short-lived biexcitons would likely explain the difficulty in achieving BEC of excitons in this crystal.

Our model contains three physical parameters, a capture coefficient $\bar{C}$, a biexciton Auger lifetime τ_A, and a biexciton binding energy ϕ, all of which must be determined experimentally over a wide range of temperatures and gas densities. To complicate matters, the exciton gas temperature T may differ from the lattice temperature T_L. There are two distinct regimes: (i) a "high-T_L" range (above about 50 K) in which the exciton gas temperature equals the lattice temperature, and the relative densities of ortho- and paraexcitons are given by the Boltzmann ratio $n_o/n_p=3e^{-\Delta/k_BT}$, where $\Delta=12$ meV is the ortho-para splitting; and (ii) a "low-T_L" range (below about 20 K) in which the effective temperature of the gas can easily differ from that of the lattice, and n_o/n_p is not the thermal equilibrium ratio. The basic question is whether there is a realistic and unique set of values for the physical parameters that explains the highly nonexponential exciton decays over the widely varying experimental conditions. For example, we must explain the huge temperature dependence of orthoexciton decay shown in Fig. 1(b).

This paper is organized as follows: In Sec. II we provide a theoretical basis for the formation and decay of biexcitons. Section III examines the approach to chemical equilibrium between excitons and biexcitons, allowing us to analyze the exciton transients under a biexciton Auger process. In Sec. IV we explain the experimental methods used to measure the exciton capture rate and biexciton properties. Noting several pitfalls that must be avoided in the high-T_L measurements, we report the photoluminescence spectra and spatial imaging of orthoexcitons at high temperatures. In Sec. V the orthoexciton temporal behaviors at high-T_L are modeled with physical parameters $\bar{C}(T)$, $\tau_A(T)$, and ϕ. In Sec. VI we analyze the low-T_L decay and buildup of both ortho- and paraexcitons using three-component rate equations. The consistency of the biexciton model is checked with the high-temperature data, providing capture and Auger rates over the temperature range 2–212 K. Section VII gives our summary and conclusions.

II. BIEXCITON FORMATION AND AUGER DECAY—THEORETICAL CONSIDERATIONS

What does theory say about the existence of biexcitons in Cu_2O? A variational calculation by Brinkman *et al.*[21] yields a biexciton binding energy of 3.3 meV. In contrast, Huang[22] applied a Feynman's path-integral approach to the biexciton problem in general. For an electron-hole mass ratio of $m_h/m_e=0.58$ for Cu_2O,[23] we find that Huang's Fig. 1 predicts a biexciton binding energy of $\phi\simeq 13$ meV. A comparison of the variational and path-integral methods for various direct-gap semiconductors seems to favor the latter approach, as illustrated in Table 5 of Ref. 24. For example, a variational calculation predicts a biexciton binding energy of 11 meV in CuCl, whereas a path-integral calculation yields 30 meV.

The measured biexciton binding energy in CuCl is 29 meV.

Although these calculations predict the stability of biexcitons in Cu_2O, no spectroscopic proof of biexcitons exists. In view of this fact, Bassani and Rovere[25] considered the role of electron-hole exchange in the stability of the biexciton in Cu_2O. They calculated an electron-hole exchange correction of −3.1 meV, although this value likely depends on the exchange parameter J used in the study. Applied to the variational result of 3.3 meV, this implies a biexciton binding energy $\phi \leqslant 0.2$ meV. If their exchange correction is applied to $\phi = 13$ meV from the path-integral method, the predicted binding energy would be about 10 meV.

We will consider how data such as those in Fig. 1 may be analyzed in terms of the binding of two excitons into a biexciton that rapidly decays by Auger recombination. A short Auger decay time compared to the binding time means that the excitons and biexcitons do not in general reach a chemical equilibrium; therefore the exciton loss rate is governed mainly by their rate of binding (i.e., "capture") into biexcitons. Considering the high-T_L regime in which the ratio of ortho and para densities is fixed, we define $n = n_o + n_p$ as the exciton gas density and n_b as the biexciton density. Following a short excitation pulse that produces the *excitons*, $n(t)$ and $n_b(t)$ are described by two simultaneous rate equations,

$$\frac{dn}{dt} = -\frac{n}{\tau} + \frac{n_b}{\tau_A} - 2\bar{C}n^2 + 2\bar{C}n^* n_b, \tag{2}$$

$$\frac{dn_b}{dt} = -\frac{n_b}{\tau_A} + \bar{C}n^2 - \bar{C}n^* n_b, \tag{3}$$

where $\bar{C}$ is the average capture coefficient defined below, τ_A is the biexciton lifetime, τ is the impurity-limited lifetime of an exciton, and $n_b(0) = 0$. For nondegenerate exciton and biexciton ground states,[26] the mass-action equilibrium density is given by

$$n^*(T) = \frac{n^2}{n_b} = \left(\frac{mk_BT}{4\pi\hbar^2}\right)^{3/2} e^{-\phi/k_BT}, \tag{4}$$

where the biexciton mass is assumed to be twice as large as a free exciton mass m, and ϕ is the binding energy of a biexciton. A plot of n^* for several values of ϕ is shown in Fig. 2. Equation (3) assumes that the impurity-induced lifetime of biexcitons is much longer than the Auger lifetime τ_A.

We can estimate the magnitude of the capture coefficient by noticing that immediately after a strong excitation pulse, the term $2\bar{C}n^2$ in Eq. (2) gives the instantaneous decay rate, similar to the An^2 term in Eq. (1), which was used to determine $A_{\text{expt}} \simeq 10^{-16}$ cm^3/ns at a temperature of 70 K. (The factor of 2 arises because, unlike Auger decay, the capture process does not produce a hot e-h pair that rapidly cools to an exciton.) Thus $2\bar{C} \simeq 10^{-16}$ cm^3/ns at this temperature. Neglecting backflow due to both biexciton dissociation ($2\bar{C}n^* n_b$) and Auger (n_b/τ_A) processes at 70 K, we find a scattering cross section $\sigma = \bar{C}/v = 2 \times 10^{-14}$ cm^2, which is comparable to $4\pi a_B^2 = 6 \times 10^{-14}$ cm^2, using the exciton Bohr radius $a_B = 7$ Å.

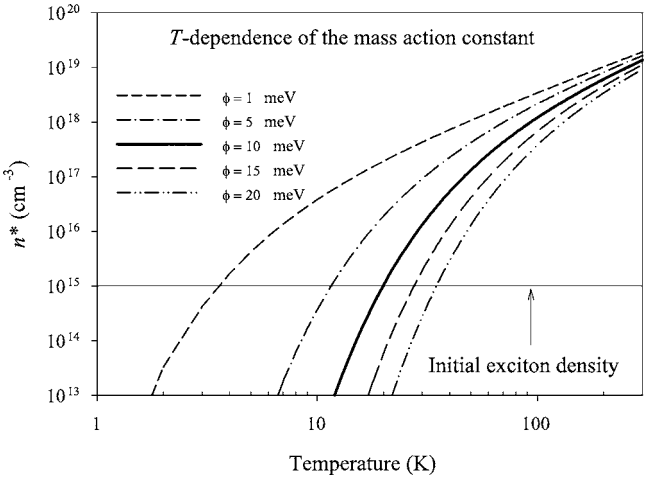

FIG. 2. Temperature dependence of the mass action density $n^*(T)$ for several biexciton binding energies $1 < \phi < 20$ meV. For chemical equilibrium the exciton density is larger than the biexciton density when n^* is larger than the exciton density n, which is initially 10^{15} cm^{-3} in our experiments. For $\phi = 10$ meV, this crossover occurs around $T = 20$ K.

Most important, if biexcitons are energetically stable the capture coefficient can be much larger than an exciton Auger constant because A involves recombination in this forbidden direct-gap crystal, whereas $\bar{C}$ does not. Unlike the exciton Auger constant that theoretically increases with increasing temperature,[16] the capture coefficient is expected to decrease with increasing gas temperature because rapidly moving excitons are less likely to form biexcitons.

Orthoexcitons and paraexcitons are expected to have different capture coefficients due to their spin value. The average capture coefficient in Eqs. (2) and (3) is defined by

$$\bar{C}n^2 = C_o n_o^2 + 2C_{op} n_o n_p + C_p n_p^2. \tag{5}$$

We expect that biexcitons will be created in their "para-para" ground state either by the binding of two paraexcitons or by two orthoexcitons of opposite spin alignment;[27] therefore we set $C_o = C_p/3$ and $C_{op} = 0$, which yields the more tractable relation

$$\bar{C}n^2 = C_o n_o^2 + C_p n_p^2 = C_p(n_o^2/3 + n_p^2). \tag{6}$$

For a specific $T_L \geqslant 50$ K, the ratio n_o/n_p is constant during a luminescence transient, so $\bar{C}$ and C_p are constants in Fig. 1(a). At low T_L, densities n_o, n_p, and gas temperature T change with time, making the analysis a little more difficult, as considered in Sec. VI. With these simplifying assumptions, only a single capture coefficient $C_p(T)$ is required to cover the entire temperature range.

How strong is a biexciton Auger decay rate $\tau_A^{-1}(T)$ and what is its temperature dependence? We consider here only the direct process,[28] as opposed to the phonon-assisted process.[15] Because the biexciton wave function is unknown, we cannot directly calculate its Auger decay rate. Nevertheless, in order to predict how this rate depends on temperature, we apply the Auger theory of Kavoulakis and Baym[16]

to a hypothetical biexciton bound by the van der Waals (vdW) interaction. In this case, the effective volume of a biexciton is approximately $(E_x/\phi)a_B^3$, where $E_x=153$ meV is the binding energy of an exciton. The matrix element for the direct Auger process is given by[18]

$$M_A \simeq -\frac{4\pi e^2}{\Omega\epsilon K^2}\mathbf{K}\cdot\left(\frac{\partial\phi_{\mathbf{k}_e}}{\partial\mathbf{k}_e}\right)\sum_{\mathbf{q}}\phi_{\mathbf{q}}\langle u^v_{\mathbf{q}-\mathbf{K}/2}|u^c_{\mathbf{q}+\mathbf{K}/2}\rangle, \quad (7)$$

where Ω is the crystal volume, $\mathbf{K}$ is the initial center-of-mass momentum of a biexciton, and $\mathbf{k}_e\simeq-\mathbf{k}_h$ are the final momenta of the ionized electron and hole. In Eq. (7) $\phi_{\mathbf{q}}$ is the Fourier transform of $1s$-hydrogenic wave function and $u^j_{\mathbf{p}}$ is an atomic wave function with band index j (=conduction or valence) and momentum $\mathbf{p}$.

The direct Auger process is forbidden at $\mathbf{K}=0$ due to band orthogonality and is allowed only for nonzero kinetic energy. The $\mathbf{k}\cdot\mathbf{p}$ calculation of the band overlap integral $\langle u^v_{\mathbf{q}-\mathbf{K}/2}|u^c_{\mathbf{q}+\mathbf{K}/2}\rangle\propto K^2$ leads to a matrix element M_A proportional to K. Since the density of the final states is insensitive to the initial momentum of a biexciton, the direct Auger rate at a gas temperature T is proportional to the matrix element squared:[29]

$$\frac{1}{\tau_A(T)}\simeq\frac{k_BT}{2^{-16}\hbar}E_x^2\frac{(n_{\text{eff}}a_B^3)(k_ga_B)^3}{[1+(k_ga_B)^2]^6}\left(\frac{|\mathbf{p}_{c'c}||\mathbf{p}_{c'v}|}{m_eE^c_{c'}E^v_{c'}}\right)^2, \quad (8)$$

where k_g is defined as $E_{gap}=\hbar^2k_g^2/2\mu$ with a reduced mass of electron and hole μ, the energy denominator $E^i_{c'}$ is the energy difference between the $i=\Gamma_6^+$ conduction (or Γ_7^+ valence) band, and the negative parity c' conduction band, which is 0.5 eV higher than the Γ_6^+ conduction band. The matrix element of the dipole moment operator is given by $|\mathbf{p}_{c'v(c)}|/\hbar=0.13$ Å^{-1}.[30] The effective density n_{eff} is the inverse of the biexciton volume. Within the vdW-biexciton picture, the predicted Auger lifetime is about 650 ps at 212 K. This simple estimate is considerably longer than the 10 ps obtained experimentally, but the assumptions of a vdW wave function and the dependence of A on high powers of the Bohr radius and the dipole transition matrix element introduce many numerical uncertainties.[18]

Most importantly, Eq. (8) predicts a linear temperature dependence of Auger rate $\tau_A^{-1}(T)=aT$. At zero kinetic energy there is no Auger recombination of biexcitons due to band orthogonality. As seen above, the Auger rate increases with the biexciton kinetic energy, which is proportional to the temperature of the biexciton gas.

III. CHEMICAL EQUILIBRIUM AND AUGER DECAY—AN OVERVIEW

The physical parameters $C_p(T)$, $\tau_A(T)$, and ϕ cannot be completely determined solely in the low-T_L or high-T_L regimes. Both temperature regimes are required. We can understand the problem by considering a numerical example of the gas dynamics. Assume a biexciton binding energy $\phi=10$ meV, and a capture coefficient $\bar{C}=10^{-16}$ cm^3/ns at $T_L=70$ K. How does the biexciton Auger rate affect the particle decay following an excitation pulse that produces an initial exciton density $n(0)=10^{15}$ cm^{-3} and an initial biexciton density $n_b(0)=0$?

Consider Eqs. (2)–(4) governing the densities of excitons and biexcitons, ignoring for the moment the distinction between ortho- and paraexcitons. In the limit $\tau_A^{-1}=0$, the temporal behavior of excitons is given by

$$\frac{dn}{dt}=-\frac{n}{\tau}-2\bar{C}n^2+2\bar{C}n^*n_b \text{ (no Auger process)}. \quad (9)$$

Equation (4) and Fig. 2 show that the mass-action density at 70 K has the value $n^*\simeq5\times10^{17}$ cm^{-3}. Biexcitons in chemical equilibrium with the exciton gas at $n=10^{15}$ cm^{-3} have a density of $n_b=n^2/n^*\simeq2\times10^{11}$ cm^{-3}, showing that the excitons are by far the dominant species at this temperature. Biexcitons are initially formed at a rate of $\bar{C}n^2=10^{14}$/cm^3 ns, implying that chemical equilibrium should be achieved in less than a nanosecond. For chemical equilibrium the last two terms in Eq. (9) (i.e., the formation and dissociation rates of biexcitons) cancel because $n^*=n^2/n_b$, leaving the excitons to decay with their impurity-induced lifetime τ. This single-exponential decay at $t>1$ ns is indeed predicted by numerical solution of the rate equations and is shown as the light solid line in Fig. 3(a).

In contrast, at 10 K the mass-action density n^* is less than 10^{12} cm^{-3} and it continues to decrease exponentially with a further reduction in temperature. In this case, the dissociation rate of biexcitons, $2\bar{C}n^*n_b$, is negligible, simplifying the exciton equation to

$$\frac{dn}{dt}=-\frac{n}{\tau}-2\bar{C}n^2 \text{ (no Auger process)}, \quad (10)$$

which has the same form as that for the exciton Auger decay [Eq. (1)], with the correspondence $A\rightarrow2\bar{C}$. Numerical solution of this equation yields the heavy solid curve in Fig. 3(a).

If we now increase the Auger rate from zero, the n/τ_A terms in Eqs. (2) and (3) become effective. In the limit of large τ_A^{-1}, Eq. (2) becomes $dn/dt=-n/\tau-\bar{C}n^2$ because the capture of *two* excitons is partially counteracted by the creation of *one* exciton in the subsequent Auger decay of a biexciton $(-2\bar{C}n^2+\bar{C}n^2=-\bar{C}n^2)$. The dashed curve in Fig. 3(a) represents the solution to $dn/dt=-n/\tau-\bar{C}n^2$ using the same value of $\bar{C}$ and τ as in the $\tau_A^{-1}=0$ case. Thus, even without knowing τ_A, a measurement of $n(t)$ at low temperatures (when n^* terms are negligible) provides a value of the capture coefficient within a factor of 2. A constraint on the value of the Auger rate is extracted from the orthoexciton and paraexciton transients, as described in Sec. VI, Appendix B, and Ref. 31. Because the n^* terms do not enter into this analysis, the biexciton binding energy cannot be determined from the low-T_L data.

One of our principal results is that $C_p(T)=c/T$ with a "best-fit" capture constant $c_m=(1.4\pm0.4)\times10^{-14}$ K cm^3/ns is consistent with our data over the entire temperature range. Indeed there is only a small range of capture constants that are in acceptable agreement with all the experimental data.

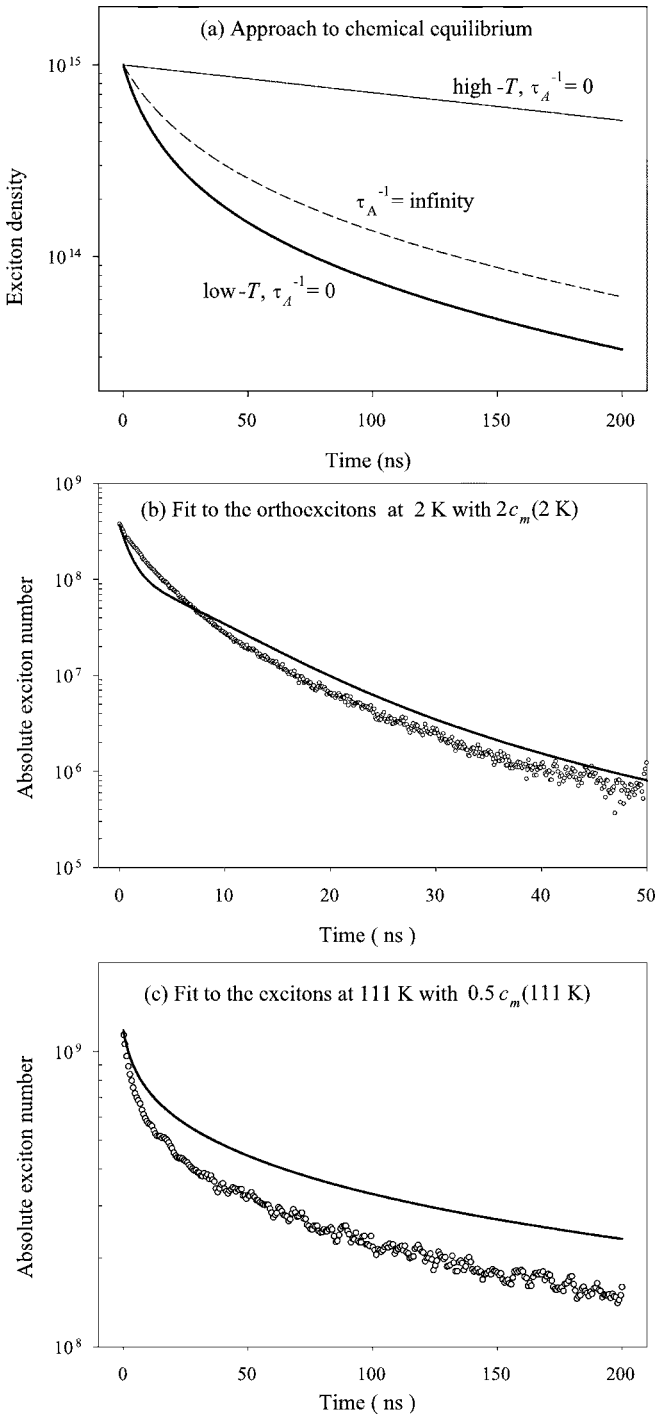

FIG. 3. (a) Predicted exciton transients obtained by assuming the exciton-biexciton equilibrium dynamics. To illustrate the effect of chemical equilibrium, we have neglected the T dependence of $\bar{C}$ and choose $\bar{C}=10^{-16}$ cm^3/ns. The solid curves correspond to $\tau_A^{-1}=0$ in low- and high-T limits, where biexcitons and excitons are the dominant species, respectively. The dashed curve is described in the text. (b) Best fit to the observed orthoexciton transient at $T_L=2$ K assuming $c=2c_m$. (c) Best fit to the observed exciton transient at $T_L=111$ K assuming $c=c_m/2$. The restriction on the main fit parameter is deduced from these notable deviations from the experiments.

Figures 3(b) and 3(c) show fits to the data for the choices $c=2c_m$ at $T_L=2$ K and $c=c_m/2$ at $T_L=111$ K, allowing full degree of freedom in the other two parameters, τ_A and ϕ. Based on such comparisons (including much better fits for $c=c_m$), we can confidently restrict the range of capture constants to $0.8c_m<c<2c_m$.

We begin our data analysis at high-T_L, using $c=c_m$, and determine both the biexciton binding energy ϕ and the biexciton Auger rate $\tau_A^{-1}=aT$. Finally we will demonstrate that our low-T_L data is consistent with all three of these parameters (c, a, and ϕ). First we describe the special features of the measurements, which involve absolute calibration of exciton number by their luminescence intensity, spatial measurements of the expanding gas volume, and time decays of both excitonic species under a broad range of conditions.

IV. PHOTOLUMINESCENCE MEASUREMENTS AT $T_L>70$ K

To create a high density of excitons in a controlled volume, we optically excite with a cavity-dumped dye laser that is synchronously pumped by a mode-locked YLF laser. The system produces 5-ps pulses at a repetition rate of 4.75 MHz and an average power up to 30 mW, corresponding to about 10^9 photons/pulse incident on the sample. The full width at half maximum of the focused beam is about 30 μm, and the wavelength is adjusted to produce an absorption length in the sample of about 100 μm in order to minimize the effects of surface recombination. Each dot in Fig. 4(b) indicates the selected absorption length ranging from 90 to 130 μm for each temperature.

Photoluminescence is detected from the Γ_{12}^- phonon-assisted orthoexciton line. For $t\geqslant 1$ ns, the orthoexciton spectra are well described by a Maxwell-Boltzmann (MB) distribution at the lattice temperature. Earlier results[32] showed that on this time scale the paraexcitons have reached thermal equilibrium with the lattice. Typical orthoexciton spectra are shown in Figs. 4(a) and 5(a).

Figure 4 illustrates how the absorption of luminescence light in the crystal can cause an inaccurate measurement of the exciton gas temperature. The inset to part (a) shows our experimental configuration with luminescence light collected at right angles to the laser beam. Also plotted are the photoluminescence spectra for two positions of the laser beam. The combined fit of the phonon-emission (Stokes) and phonon-absorption (anti-Stokes) components can be used to determine the distance of the exciton cloud from the surface facing the spectrometer. If the exciton cloud is produced 150 ± 10 μm from this surface, the Stokes spectrum shows a kinetic energy distribution (spectrum A, circles) that is nearly the same as a Maxwell-Boltzmann (MB) fit (spectrum A') at the lattice temperature of $T_L=120$ K.

If the exciton cloud is created 150 ± 10 μm from the *opposite* surface of the sample, the apparent fit temperature is 55 K (spectrum B, dots). To extract the actual kinetic energy distribution from the spectrum B, we would need to multiply it by $\exp[\alpha(h\nu,T_L)d]$, where $\alpha(h\nu,T_L)$ is the absorption coefficient of the crystal, $h\nu$ is the photon energy, and $d\simeq 2$ mm is the distance between the exciton cloud and the

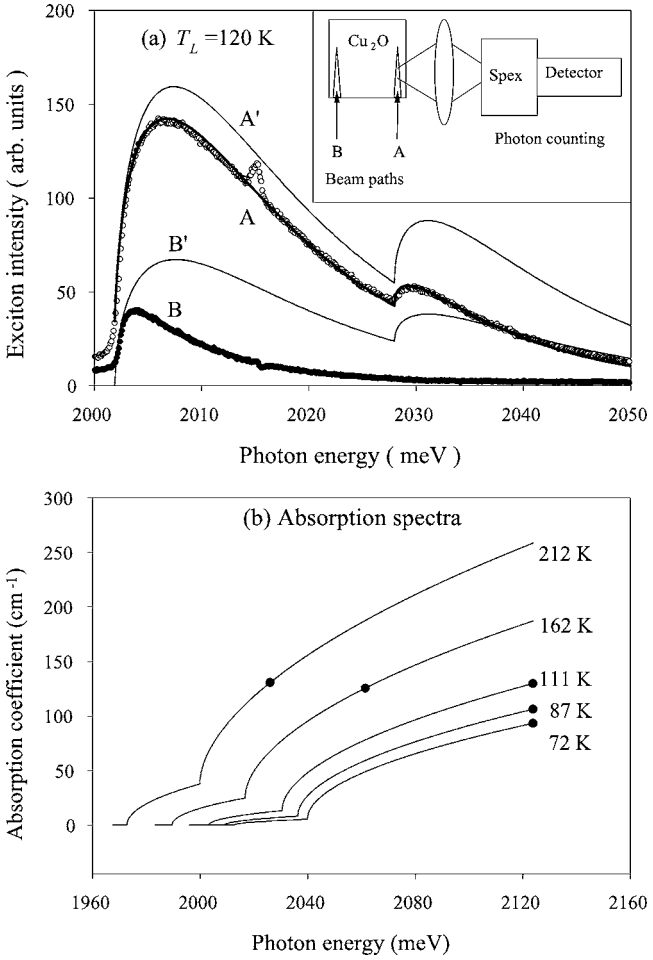

FIG. 4. (a) Time-integrated luminescence of orthoexcitons at T_L=120 K for the two different excitation positions. The inset shows a schematic diagram of the collection geometry. For laser beam path A, excitons are created 150±10 μm from the surface facing the spectrometer maximizing the primary exciton signal. Exciton luminescence with beam path B is weaker due to absorption in the crystal. Solid lines labeled A′ and B′ are classical Boltzmann fits at T_L=120 K with different normalization constants. Multiplying A′ (or B′) by the absorption factor $\exp[-\alpha(h\nu,T_L)d]$ yields the predicted spectrum A (or B), which agrees with the data. (b) The Γ_{12}^{-} phonon-assisted absorption spectra calculated with $\alpha(h\nu)=8(h\nu)^{1/2}$ cm^{-1}, where $h\nu$ is in meV.[10] Each dot indicates the excitation energy for a given temperature, chosen to keep an absorption length d=90–130 μm.

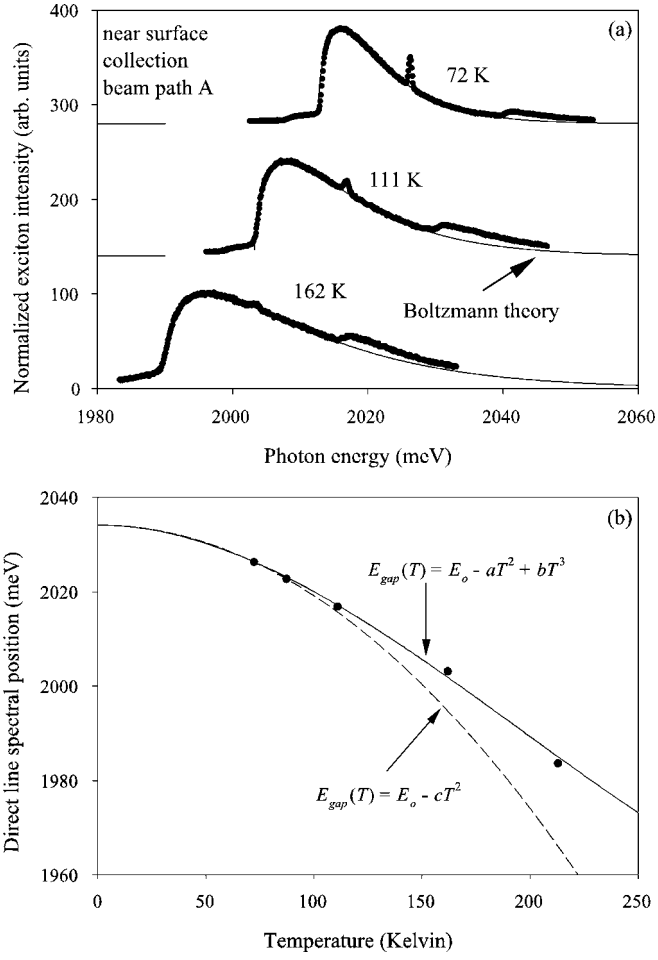

FIG. 5. (a) Normalized time-integrated Γ_{12}^{-} phonon-assisted orthoexciton luminescence at T_L=72, 111, and 162 K by near-surface collection, also using spatial filtering. The solid curves are corresponding MB functions at the measured bath temperatures. For an accurate fit to the data and estimate of d, the strong Stokes absorption band seen in Fig. 4(b) must be accounted for. (b) Redshift of the band-gap energy at increasing temperature. The dashed curve shows a second-order fit with E_o=2034.13 meV and c =0.0015 meV/K^2. The solid curve is our third-order fit (Ref. 33).

collection face. As expected, the result is consistent with the 120-K theory labeled B' in Fig. 4(a).

Obviously the best procedure is to place the exciton cloud near the collection surface, which we do throughout the high-temperature experiments (T_L>70 K). About 150 μm from the collection surface is optimum for maximizing transmission of the primary cloud with negligible loss of excitons due to nonradiative surface recombination. Figure 5(a) shows that the luminescence collected through the nearby surface yields spectra in good accord with MB functions at each lattice temperature where only Stokes-line fits are shown for simplicity. Figure 5(b) shows the measured band-gap shifts[33] as a function of temperature, which is essential in determining $\alpha(h\nu,T_L)$.

"Secondary excitons," created by absorption of luminescence light, emit a diffuse background of luminescence that displays a much different temporal character from that of the "primary excitons." Fortunately, emission from the secondary excitons can be subtracted from that of the primary excitons by employing a procedure that we call "spatial filtering." By slightly translating the image of the crystal on the spectrometer slit, we obtain signals "on" and "off" the primary cloud of excitons. Subtracting "off" from "on" signals, we observe only the dynamics of the primary (dense) cloud of excitons. This procedure is essential to a determination of $\bar{C}(T)$ at $T_L \geqslant 70$ K because the secondary luminescence is comparable to, or greater than, the primary luminescence.

The secondary emission is actually useful for determining the lifetime $\tau(T)$ of excitons due to nonradiative recombination at impurities,[34] which can vary among samples. The

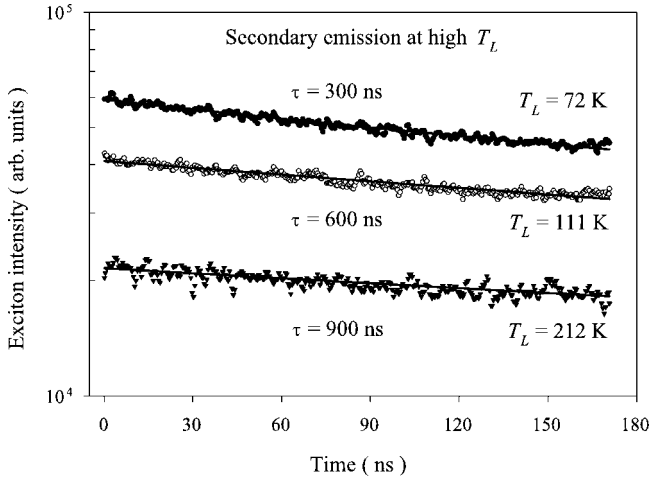

FIG. 6. Luminescence decays of the low-density gas giving the impurity-induced recombination times $\tau(T)$ at T_L=72, 111, and 212 K.

present experiments are conducted with a high-purity natural-growth crystal[35] that was cut from a sample provided by the Smithsonian Institute—the same crystal used in Refs. 32 and 36. Figure 6 shows typical impurity-induced decays at three temperatures in our experimental range, allowing us to eliminate $\tau(T)$ as a fitting parameter in Eqs. (2) and (3).

Also, we must account for the fact that the measured number of luminescence photons emitted depends on the lattice temperature. The measured radiative rate of an exciton at T_L=2 K is about $\gamma_{12} \simeq 7 \times 10^4$/s.[10] At temperatures above about 70 K stimulated emission begins to contribute significantly, which can lead to an overestimate of the actual number of excitons. For example, the Γ_{12}^- optical phonon occupation number $f_{12}(T_L)$ at 212 K is about 0.9, causing almost a factor of 2 increase in the luminescence intensity for a given number of excitons.

By translating an image of the crystal across the entrance slit of the spectrometer, the number of excitons being sampled $N(x,t)dx$ is measured. The photon counting system has a 70-ps time response and the optical resolution is about σ_s=3 μm. Figure 7(a) shows "spatial profiles" of the exciton luminescence for various times after the excitation pulse. These data are obtained by setting the spectrometer wavelength on the peak of the orthoexciton line and then scanning the image of the crystal across the entrance slit of the spectrometer. A close look at these data shows that the intensity at the center of the cloud falls much faster than the intensity in the tails. This is a signature of a density-dependent capture effect, the instantaneous decay rate being proportional to the gas density. A consequence of the inhomogeneous decay rate is that the width of the spatial distribution (defined by the standard deviation σ) increases in time—an effect that has previously been called "Auger broadening."[10,11] In this paper, in view of the new interpretation involving biexcitons, we use the terminology "capture broadening."

Capture broadening is characterized by plotting σ^2 as a function of time, shown in Fig. 7(b). During the first 50 ns or so, a rapid nondiffusive expansion in the cloud width is caused by a stronger recombination in the center of the cloud

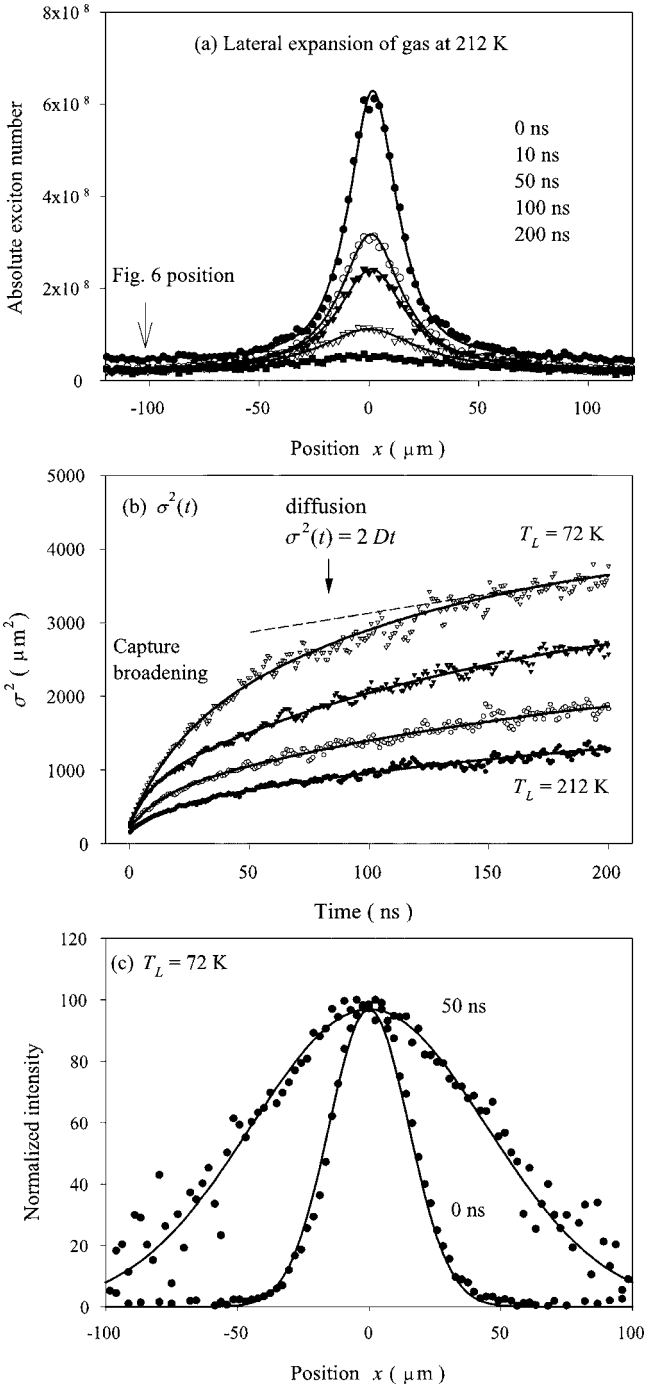

FIG. 7. (a) Time-resolved spatial profiles at T_L=212 K. These are well described by 2D Gaussian distributions shown as the solid curves. The capture process is most effective at the center of the distribution, causing an apparent expansion ("capture broadening") that modifies the effective volume of the exciton cloud. (b) The square of the Gaussian width as a function of time for T_L=72, 111, 162, and 212 K. The capture broadening is significant for t < 50 ns. The late-time expansion is caused by exciton diffusion. The solid curves are parametric fits to the data given by $\sigma^2(t) = \sigma_o^2 - ae^{-bt} - ce^{-dt}$. (c) Normalized spatial profiles, superimposed by corresponding Gaussian fits at T_L=72 K for t=0 and 50 ns.

as biexcitons are formed and decay. At $t>100$ ns the increase in cloud size has a diffusive form $\sigma^2(t)=2Dt$. The observed diffusion constants are consistent with earlier measurements.[36] The experimental data clearly demonstrate that the capture broadening is more significant at lower temperatures. The spatial profiles are well approximated by Gaussian distributions throughout the expansion process; therefore the measured standard deviation $\sigma(t)$ (and its counterpart normal to the excitation surface) may be used to parametrize the effective volume $V(t)$. The shape of the exciton cloud normal to the excitation surface is shown in Appendix A, along with a quantitative analysis of $V(t)$.

To better understand why it is so important to account for the capture-broadening effect, consider Fig. 7(c). Spatial profiles at $T_L=72$ K for $t=0$ and 50 ns are normalized to the same height. Neither the intensities at the peak of the distribution nor the total integrated intensities are measures of the effective gas densities, $n(t)=N(t)/V(t)$. Both $N(t)$ and $V(t)$ must be measured.

V. EXCITON/BIEXCITON KINETICS AT $T_L=72-212$ K

Consider first the high-T_L regime (above about 50 K) in which the exciton kinetic energies reach thermal equilibrium with the lattice on a subnanosecond time scale. At observation times greater than a nanosecond the ratio of ortho- and paraexcitons is determined by Boltzmann statistics at the lattice temperature. Thus at a given temperature the total exciton number $N(t)$ can be determined from the orthoexciton number $N_o(t)$, which is obtained from the spectrally and spatially integrated luminescence. With the measured initial exciton number $N(0)$, the effective volume $V(t)$, and the residual decay time τ, the "local" rate equations (2) and (3) become

$$\frac{dN}{dt}=-\frac{N}{\tau}+\frac{N_b}{\tau_A(T)}-2\frac{\bar{C}(T)}{V(t)}N^2+2\bar{C}(T)n^*N_b, \qquad (11)$$

$$\frac{dN_b}{dt}=-\frac{N_b}{\tau_A(T)}+\frac{\bar{C}(T)}{V(t)}N^2-\bar{C}(T)n^*N_b, \qquad (12)$$

where $\bar{C}(T)=C_p(T)(N_o^2/3+N_p^2)/N^2$. Note that $\bar{C}(T)$ has a slightly different T dependence from $C_p(T)=c_m/T$ due to an additional temperature dependence stemming from $N_o/N_p=3e^{-\Delta/k_BT}$. With these equations, we can predict the total exciton number $N(t)$ for various choices of capture coefficient $\bar{C}(T)$, Auger lifetime $\tau_A(T)$, and biexciton binding energy ϕ [which determines n^* from Eq. (4)].

Figure 8(a) shows a comparison of the biexciton model [based on Eqs. (11) and (12)] to the observed temporal decay of orthoexcitons at 111 K. The parameters producing the heavy solid curve are our "best fit" parameters (subscripted "m") that are consistent with data at temperatures between 2 and 212 K. The other curves show how the predictions change when τ_A^{-1} or ϕ is changed by a factor of 2, fixing the other two parameters to the best-fit values.

In Fig. 8(b) we fix the best-fit value of the capture coefficient and plot the fitted $\tau_A^{-1}(T)$ for several values of ϕ. Only

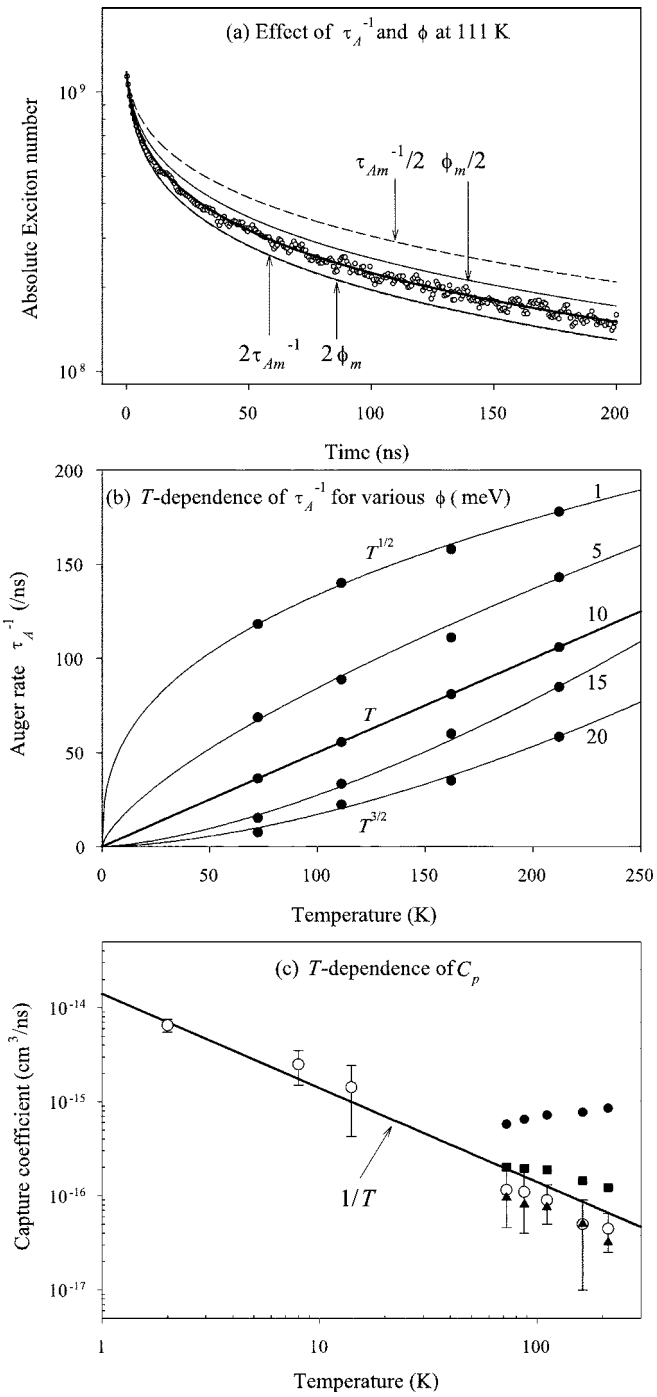

FIG. 8. (a) Exciton transient at 111 K superimposed by the best fit (heavy solid curve) with $C_p=0.9\times10^{-16}$ cm^3/ns, $\tau_{Am}^{-1}=55.5$ ns$^{-1}=a_mT$, and $\phi_m=10$ meV. The solid curves are generated by varying ϕ by factor of 2 larger and smaller while keeping other parameters fixed. Similarly, the dashed curves are obtained by changing τ_A^{-1}. Two curves nearly overlap for $2\tau_{Am}^{-1}$ and $2\phi_m$. (b) T dependence of τ_A^{-1} for $\phi=1$, 5, 10, 15, and 20 meV. For C_p given above, $\phi\simeq10$ meV yields $\tau_A^{-1}=aT$. The fits (solid curves) are empirically determined with a T^b form. (c) T dependence of $C_p(T)$ for $a=a_m/5$ (dots), $a_m/3$ (squares), and $5a_m$ (triangles) for $T_L>70$ K. Compare each with the $1/T$ dependence of $C_p(T)$ (solid line) obtained with $a_m=0.5$ ns^{-1} K^{-1} (circles).

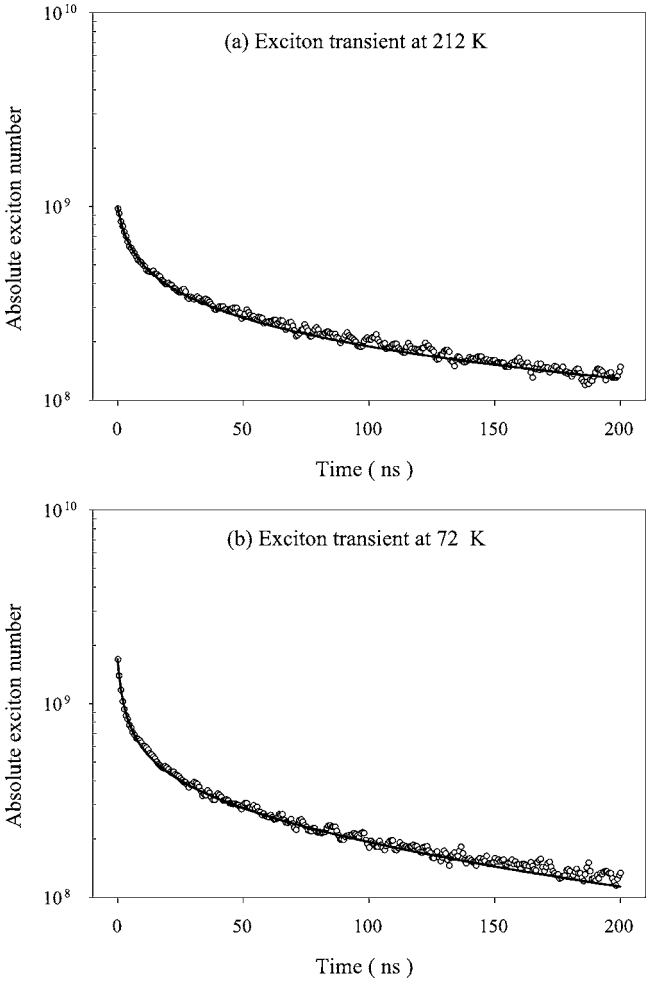

FIG. 9. Temporal behavior of the excitons at (a) T_L=72 K and (b) T_L=212 K. In both cases, solid curves are generated by Eqs. (11) and (12) using $V(t)$ from Eqs. (A6) and (A7).

ϕ=10 meV supports the linear dependence predicted in Sec. II and corresponds to $\tau_A^{-1}=0.5T$ ns^{-1} K^{-1} [the heavy solid line in Fig. 8(b)]. Varying the capture constant over the range $0.8c_m$–$2.0c_m$ discussed in Sec. III, we find a linear-T dependence in $\tau_A^{-1}(T)$ for values of ϕ between about 8 and 15 meV, which we take as the uncertainty in ϕ.[29]

Figure 8(c) shows the temperature dependence of $C_p(T)$ for several values of a in $\tau_A^{-1}=aT$. For a=0.1 ns^{-1} K^{-1} a nearly linear temperature dependence in $C_p(T)$ is obtained. In addition to yielding large uncertainties in the fitted parameters of ϕ and C_p, the resulting C_p is also inconsistent with the observed reduction in capture broadening at higher temperatures (see Fig. 7). Finally, the best-fit parameters, $\tau_{Am}^{-1}(T)=0.5T$ ns^{-1} K^{-1}=a_mT and ϕ_m=10 meV, correspond to the near $1/T$ dependence in $C_p(T)$, as shown by the open circles in Fig. 8(c). In this plot we have included data at low T, which uses these same parameters, as explained in the next section.

Figure 9 shows exciton transients at T_L=72 and 212 K, bracketing our high-T range. The initial decay rates are primarily due to the exciton capture and biexciton Auger recombination processes. As the density falls, the instantaneous decay rate depends on the combined effects of biexciton dissociation and Auger decay. With $\tau_{Am}^{-1}(T)=0.5T$ ns^{-1} K^{-1} and ϕ_m=10 meV, we fit the exciton transients by only adjusting $\bar{C}(T)$ [or equivalently $C_p(T)$] from T_L=72 to 212 K. The solid curves in Fig. 9 are excellent fits to the experimental $N(t)$. The fits for T_L=72 and 212 K yield *average* capture coefficients of $\bar{C}(72\text{ K})=0.6\times10^{-16}$ cm^3/ns and $\bar{C}(212\text{ K})=0.1\times10^{-16}$ cm^3/ns. As discussed in Sec. II, these results correspond to paraexciton capture coefficients of $C_p(72\text{ K})=1.2\times10^{-16}$ cm^3/ns and $C_p(212\text{ K})=0.4\times10^{-16}$ cm^3/ns, showing a nearly inverse-T dependence of C_p. The C_p's obtained here are about 35% lower than given by the overall best-fit value $C_p(T)=c_m/T$, indicating the uncertainties in C_p over the wide temperature range.

VI. RESULTS AT LOW TEMPERATURES (T_L=2–14 K)

The weak paraexciton luminescence becomes observable for experimental temperatures between 2 and 14 K. We increase the repetition rate by a factor of 2 to 9.5 MHz in order to improve the signal-to-noise ratio. The excitation wavelength is adjusted to 576 nm, producing an absorption length in the sample of about 85 μm. For these temperatures the slower phonon-assisted down-conversion rates make the analysis more complicated, although the up-conversion of paraexcitons to orthoexcitons is negligible. Photoluminescence of ortho- and paraexcitons are detected from the Γ_{12}^- phonon-assisted orthoexciton line and Γ_{25}^- phonon-assisted paraexciton line, respectively. The paraexciton signal is 500 times weaker than that of orthoexcitons at the same density. The methods used to detect the weak paraexciton luminescence are described in Ref. 32.

Because the biexciton dissociation is negligible, the three-component gas system is described by the following rate equations:

$$\frac{dn_o}{dt}=-\frac{n_o}{\tau}+\frac{3}{4}\frac{n_b}{\tau_A}-2Bn_o^2-Dn_o-2C_on_o^2,$$

$$\frac{dn_p}{dt}=-\frac{n_p}{\tau}+\frac{1}{4}\frac{n_b}{\tau_A}+2Bn_o^2+Dn_o-2C_pn_p^2,$$

$$\frac{dn_b}{dt}=-\frac{n_b}{\tau_A}+C_on_o^2+C_pn_p^2, \tag{13}$$

where D is the phonon-assisted down-conversion rate and B is the density-dependent spin-flip constant.[37] Note that if dn_o/dt and dn_p/dt are added the above simultaneous equations reduce to Eqs. (2) and (3) with $n^*(T)=0$. In this model we assume that an orthobiexciton formed by the ortho-ortho capture quickly decays into a lower-lying parabiexciton by the internal mutual spin flip (Bn_{eff}),[38] where n_{eff} is the inverse of the biexciton volume, as discussed in Sec. II.

We have previously measured the down-conversion rate $D(T_L)$ at each lattice temperature and low excitation levels,[32] eliminating it as a fit parameter. A newly introduced param-

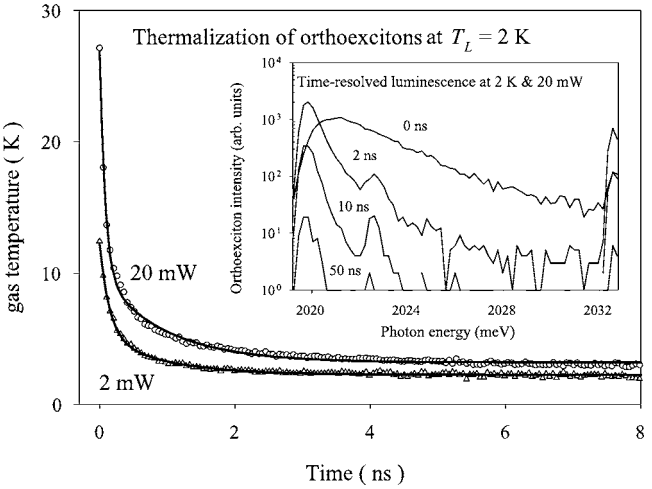

FIG. 10. Inset shows the orthoexciton kinetic energy distributions for several times after the laser pulse at T_L=2 K. A MB fit to each luminescence spectrum yields an exciton gas temperature that is plotted as a function of time. By using this with exciton volume expansion, we can infer the *gas*-temperature-dependent capture coefficient at low T_L.

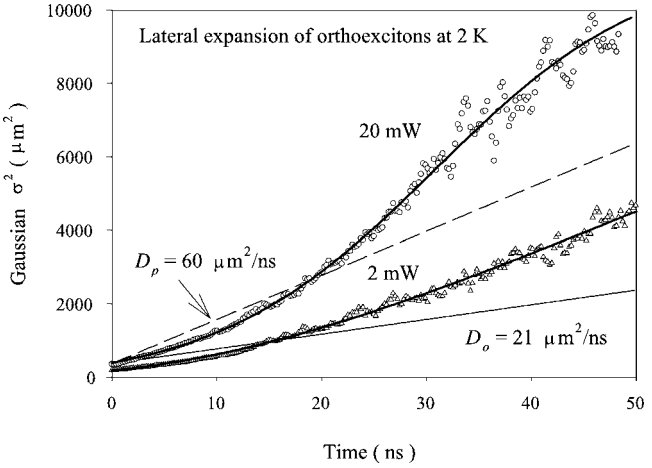

FIG. 11. Expansion of the orthoexciton gas represented by $\sigma^2(t)$ for two excitation levels, 2 mW (triangles) and 20 mW (circles) at T_L=2 K. The solid (dashed) line is the predicted expansion due to (ortho-) paraexciton diffusion. The data clearly indicate that the capture broadening is stronger for 20-mW excitation. The explanation for complicated behaviors in the orthoexciton expansion is given in the text. The solid curves are phenomenological fits to the data.

eter in Eqs. (13) is the spin-flip scattering coefficient B that converts two orthoexcitons into two paraexcitons with large kinetic energy. We use a theoretically calculated value of $B \simeq 2\times 10^{-16}$ cm^3/ns.[18,37] Using $\tau_A(T)$ determined in the previous section, the only variable fitting parameter is the temperature-dependent capture coefficient $C_p(T)$. We find that the mutual spin-flip rate Bn_o hardly affects the value of the capture coefficient $C_p(T)$.[29]

One of the complicating factors in the low-temperature experiments is that the exciton gas temperature T at times up to a couple nanoseconds varies significantly from the lattice temperature T_L. Because the capture coefficient depends on the gas temperature, we must extract the instantaneous T from the time-resolved luminescence spectra. The inset in Fig. 10 shows time-resolved orthoexciton spectra at a lattice temperature of T_L=2 K for several time delays. Notice that the orthoexciton signal is observed even at 50 ns, despite its short (3 ns) lifetime against down-conversion to paraexcitons. We believe that this effect is direct evidence for regeneration of orthoexcitons by Auger decay of biexcitons. The biexcitons are formed by capture of long-lived paraexcitons.

The biexciton Auger process also heats the exciton gas at early times. Figure 10 shows the effective gas temperature of the orthoexcitons at T_L=2 K, obtained from MB fits to the time-resolved luminescence spectra for 2 mW (triangles) and 20 mW (circles) excitation powers. The solid curves are phenomenological fits with a double exponential function, showing a slightly slower gas thermalization at higher excitation level.

At 2 K the effective volume of the gas expands much more rapidly than in the high-temperature cases of Secs. IV and V. Figure 11 shows the observed $\sigma^2(t)$ at 2 K for 2- and 20-mW excitation powers. The superimposed curves are phenomenological fits with a sigmoidal form. The solid (dashed) line corresponds to the predicted gas expansion due to orthoexciton (paraexciton) diffusion, given by $2Dt$. In Cu_2O, the paraexciton diffusion constant D_p is known to be larger than the orthoexciton diffusion constant D_o.[10] Under 20-mW excitation level, for several nanoseconds after the pulse, the width of the orthoexciton profile expands faster than its diffusion limit $2D_ot$ due to the density-dependent capture broadening. For $t>40$ ns, however, the "orthoexciton" expansion is close to that predicted by the "paraexciton" diffusion constant, implying that the regenerated orthoexcitons are produced by Auger decay of biexcitons created from the faster moving paraexcitons. The apparently fastest intermediate expansion, actually larger than both $2D_ot$ and $2D_pt$, connects the two regimes.[18] The density-dependent increases in σ^2 are not actually due to transport but to an apparent expansion from the capture broadening that is most pronounced at high densities.

We assume that the volume occupied by orthoexcitons is approximately the same as that of paraexcitons, due to rapid down-conversion and regeneration. The effective volume $V(t)$ is again calculated by considering both lateral and depth distribution (see Appendix A). We numerically solve Eqs. (13) describing the three-component gas system to fit both observed ortho- and paraexciton numbers at a given temperature and excitation power. A simultaneous fit to the ortho and para transients determines the capture coefficient $C_p(T)=3C_o(T)$ governing the initial rapid exciton loss and producing the pronounced regeneration tails at later times. Note that the numerical simulation must take into account the *time*-dependent capture coefficient $C_p(T)$ because the gas temperature is a function of time, $T(t)$, as shown in Fig. 10.

Figure 12 shows (a) the observed $N_o(t)$ for orthoexcitons and (b) the simultaneous $N_p(t)$ for paraexcitons. Superimposed on these data are the numerical solutions to Eqs. (13) (heavy solid curves) at 2 K for two different excitation levels. Assuming previously determined τ_A^{-1} (2 K)=1 ns^{-1}, the

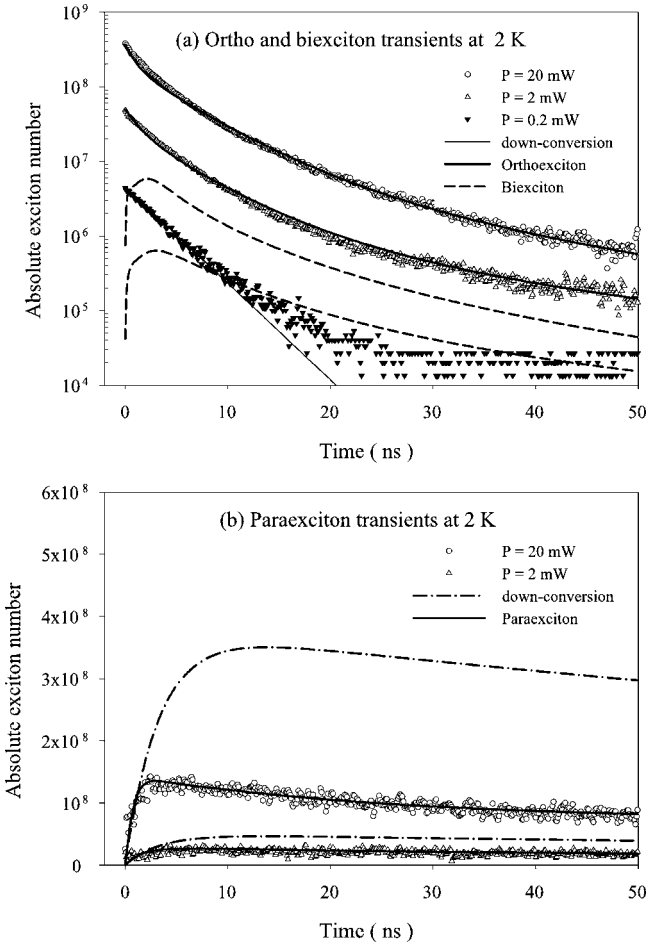

FIG. 12. (a) Orthoexciton transients at T_L=2 K. The fits (heavy solid curves) are produced by considering Figs. 10 and 11. The predicted biexciton transients for 2 and 20 mW are plotted as the dashed curves. For the lowest excitation level of 0.2 mW, the down-conversion rate is measured to be about 0.3 ns^{-1} (solid line). (b) Corresponding paraexciton transients, superimposed by simultaneous fits (heavy solid curves). The dash-dotted curves are obtained if no density-dependent process is assumed. Note the linear vertical scale in part (b).

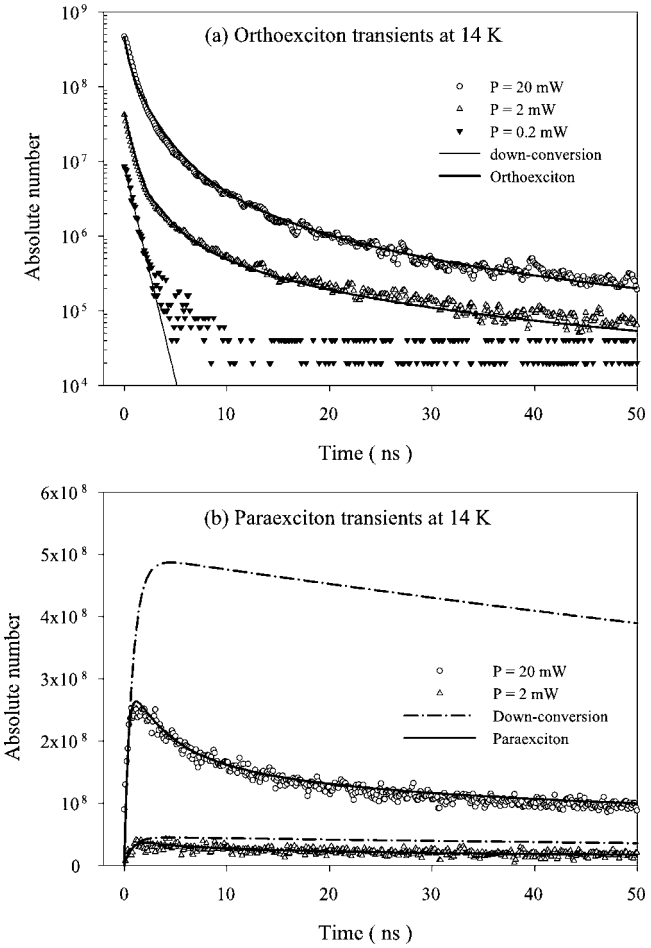

FIG. 13. (a) Orthoexciton transients at T_L=14 K. The fits are obtained with the same method as in Fig. 12. The measured down-conversion rate is about 1.3 ns^{-1}. (b) Corresponding paraexciton transients. The late orthoexciton temporal behaviors results from the biexciton Auger process.

analysis yields a fit parameter of C_p (2 K)$\simeq$6.5 $\times 10^{-15}$ cm^3/ns when the gas temperature equilibrates with the lattice temperature.[39]

The dashed curves in Fig. 12(a) are the predicted numbers of biexcitons for 2 and 20 mW. The dash-dotted curves in part (b) correspond to the paraexciton buildup if no density-dependent process (Auger) were active. Most significantly, if there were no Auger regeneration of excitons the ratio of ortho-to-para numbers would approach $3e^{-\Delta/k_BT} \simeq 10^{-30}$ at 2 K, which is many orders of magnitude smaller than the ratio observed in Fig. 12 (see also Sec. III and Fig.17 in Appendix B). The low-T_L data do not independently determine the Auger constant a, but nonzero a is required. Specifically, unacceptable fits to the data in Fig. 12 are obtained if $a<0.4$ ns^{-1} K^{-1}. Fits to the low-T_L data, however, provide no upper bound to a. (Infinite a mathematically corresponds to the exciton Auger process.)

The late temporal behavior of orthoexcitons follows that of biexcitons, which in turn is determined by the capture of paraexcitons—the dominant species. This behavior is described by the steady-state solution of Eqs. (13):

$$Dn_o = \frac{3}{4}\frac{n_b}{\tau_A} = \frac{3}{4}C_p n_p^2. \tag{14}$$

Consistent with this prediction, the late-time decay rate of both orthoexcitons and biexcitons is twice as fast as that of paraexcitons, which is limited by an impurity-limited recombination rate τ^{-1}. The down-conversion rate $D(T_L)$ at each temperature is measured at the lowest excitation level, 0.2 mW, and is represented by the light line in Fig. 12(a) for 2 K.

Figure 13 shows the observed exciton transients at 14 K. The paraexciton capture coefficient at the equilibration temperature is found to be C_p (14 K)=1.4×10^{-15} cm^3/ns. The predicted biexciton transients (not shown) are similar to those in Fig. 12. Again, the predicted biexciton numbers at late times are over an order of magnitude lower than corresponding orthoexciton numbers.

Figure 14 shows the temperature dependence of the para-para capture rate $C_p(T)n_p$ (dots) for our 2–212-K tempera-

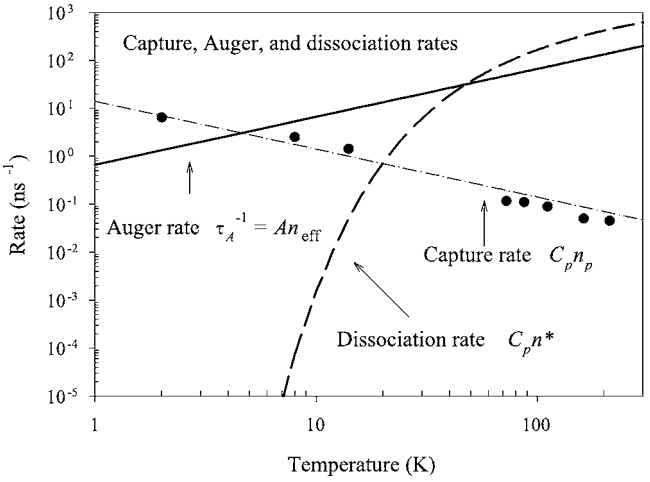

FIG. 14. Temperature dependence of the para-para capture rate $C_p(T)n_p$ (dots) assuming $n_p=10^{15}$ cm^{-3} for $T=2-212$ K. The low-temperature data points are obtained by setting $T=T_L$. The capture coefficient is approximately proportional to $1/T$ in our observation range. The dash-dotted line is obtained using Eq. (15). The solid line (dashed curve) corresponds to the temperature dependence of the Auger decay rate τ_A^{-1} (dissociation rate) from our analysis.

ture range calculated with $n_p=10^{15}$ cm^{-3}. The dash-dotted line is the best fit assuming $C_p(T)=c_m/T$ given by

$$C_p(T) \simeq \frac{(1.4 \pm 0.4) \times 10^{-14}}{T(\mathrm{K})}\ \mathrm{cm}^3/\mathrm{ns}. \tag{15}$$

Also shown are the temperature dependence of the biexciton Auger rate $\tau_A^{-1}(T)=An_{\text{eff}}=aT$ (solid line) and dissociation rate $C_p(T)n^*(T)$ (dashed curve) using C_p given by Eq. (15). We emphasize that a single set of values $\{c_m, a_m, \phi_m\}$ for the fit parameters with the T dependences shown in Fig. 14 explains the observed exciton transients at 2–212 K. The statistical uncertainty is stated in Eq. (15). An overall systematic uncertainty of a factor of 2 in the calibration of exciton density leads to a factor of 2 systematic uncertainty in C_p.

A theoretical calculation of the capture coefficient is beyond the Born approximation because the interaction is strong enough to develop the bound state of two excitons. We may compare this process with a simple two-particle scattering to form a bound state, considering the phase-shift method.[40] For low-energy scattering to form a bound state, the total cross section due to only s-wave scattering is given by

$$\sigma = \frac{2\pi\hbar^2/m_r}{E - E_b}, \tag{16}$$

where m_r is half of the exciton mass (reduced mass of two scattering particles) and $E_b=-(\hbar^2/2m_r a^2)$ is the binding energy of the final state. In this case the scattering length a is effectively the size of the bound state. The capture cross section derived from the measurement at $T_L=2$ K is about an order of magnitude larger than the cross section given by Eq. (16), implying that higher-order partial waves may contribute for some specific resonance conditions. Also the temperature dependence of the measured capture cross section $[\sigma(T)=C_p(T)/v]$ is $T^{-3/2}$, rather than T^{-1} in Eq. (16) for the high-temperature limit. Obviously, further understanding of the capture process would benefit from an advanced calculation incorporating a four-particle picture of the biexciton wave function.

VII. SUMMARY AND CONCLUSIONS

A density-dependent lifetime of excitons in Cu_2O has severely limited exciton-gas densities in attempts to achieve a thermodynamic Bose-Einstein condensation of excitons. The possibility of Auger recombination between two colliding excitons has been previously examined both experimentally and theoretically; however, the experimental lifetimes are far shorter than predicted by the existing theories.

In view of this puzzle we have examined the possibility that Auger recombination is enhanced by the formation of biexcitons. We have modeled the densities of orthoexcitons, paraexcitons, and biexcitons by three simultaneous rate equations. The model contains three physical parameters: the exciton-exciton capture coefficient $\bar{C}$ [or C_p from Eq. (6)], the biexciton Auger recombination rate τ_A^{-1}, and the biexciton binding energy ϕ. The dynamics of these particles naturally falls into two regimes: a low-temperature regime (where the three species are far from thermal and chemical equilibrium) and a high-temperature regime (where excitons and biexcitons are rapidly thermalized). Correspondingly, we have examined the exciton photoluminescence transients for lattice temperatures $T_L=2-14$ K and $T_L=72-212$ K.

Several notable complications affect the measurement of the average capture coefficient $\bar{C}$. (i) Absolute calibration of exciton densities is required, taking into account the stimulated emission of phonons at high temperatures. (ii) Above $T_L \simeq 50$ K a fraction of the luminescence from decaying excitons is reabsorbed by the crystal, producing a secondary source of low-density gas with much different temporal behavior. (iii) The capture rate depends on gas temperature, which differs significantly from the lattice temperature at $T_L \leqslant 20$ K. (iv) To determine absolute gas density it is essential to measure the effective volume of the gas, which requires controlling the absorption length of the laser and accounting for "capture broadening" of the exciton cloud.

The Auger decay of biexcitons is simpler than for two excitons because it does not depend on the gas density n_b; it depends on the biexciton wave function, which is unknown at present. In the limit of strong Auger decay of biexcitons, the density dependence of the exciton lifetime is primarily due to the capture rate. For initial exciton densities of about 10^{15} cm^{-3}, exciton capture is the primary contributor to its initial decay rate at all temperatures, although ortho-para down-conversion competes with this process at low temperatures. Theoretically the biexciton Auger rate is expected to take on a linear dependence, $\tau_A^{-1}=aT$, a relationship that is observed for binding energies in the range $\phi=8-15$ meV. Our best-fit parameters are $\tau_A^{-1}=0.5T$ ns^{-1} K^{-1}, $\phi=10$ meV, and $C_p=(1.4\times10^{-14}$ cm^3/ns K$)/T$.

Our experiments and analyses, coupled with existing theories for Auger recombination, indicate that BEC of exci-

tons is inhibited by their rapid formation of short-lived biexcitons. Our analysis also explains why biexcitons have not been observed in this crystal. Due to rapid Auger decay the predicted biexciton densities are well below those of excitons for a broad range of temperature and excitation power. On top of this, the radiative decay rate of the ground-state (para-para) biexciton in this forbidden-gap semiconductor is expected to be extremely small. Perhaps parabiexciton absorption may be observable under external stress or magnetic field. If excited-state orthobiexcitons could be created by two-photon excitation, they may decay by the spin-flip process, creating observable paraexcitons as a byproduct. Clearly there remain interesting theoretical and experimental challenges to understanding the binding and kinetics of biexcitons in Cu_2O.

ACKNOWLEDGMENTS

This work was supported in part by the U.S. Department of Energy, Division of Materials Sciences under Grant No. DEFG02-91ER45439, through the Frederick Seitz Materials Research Laboratory at the University of Illinois at Urbana-Champaign. Experiments were conducted in the MRL Laser and Spectroscopy Facility.

APPENDIX A: MODELING THE VOLUME EXPANSION

To obtain the effective volume $V(t)$ for the expanding nonuniform exciton cloud of local density $n(\mathbf{r},t)$, we integrate over spatial inhomogeneities. In Eqs. (11) and (12), the effective volume $V(t)$ is defined by

$$V(t) = \frac{\left[\int n(\mathbf{r},t)d^3\mathbf{r}\right]^2}{\int n^2(\mathbf{r},t)d^3\mathbf{r}}. \tag{A1}$$

In order to determine the effective volume $V(t)$, one must observe the spatial distribution of excitons as a function of time, both laterally and along the laser beam, as shown in Figs. 7 and 15. As illustrated in Fig. 7(a), the lateral distribution of excitons in the xy plane is well characterized by two-dimensional (2D) Gaussian distributions,

$$n(x,y,t) = \frac{N(t)}{2\pi\sigma^2(t)} e^{-(x^2+y^2)/2\sigma^2(t)}. \tag{A2}$$

In Fig. 7(b) we plot $\sigma^2(t)$ at each temperature, superimposed by solid curves that are phenomenological fits of the form $\sigma^2(t)=\sigma_o^2-ae^{-bt}-ce^{-dt}$. The fits take into account the nearly spatially invariant background signals, partly from the remnant excitons created by previous pulses but mostly from the secondary luminescence. Note that the capture broadening is more significant at lower temperatures.

Figure 15 shows the depth distribution of the exciton cloud as a function of time after the pulse. Initially the depth profile along the z direction is described by a single exponential determined by the absorption length d of the laser. If the shape of depth profile remained constant, then the exciton density would be given by

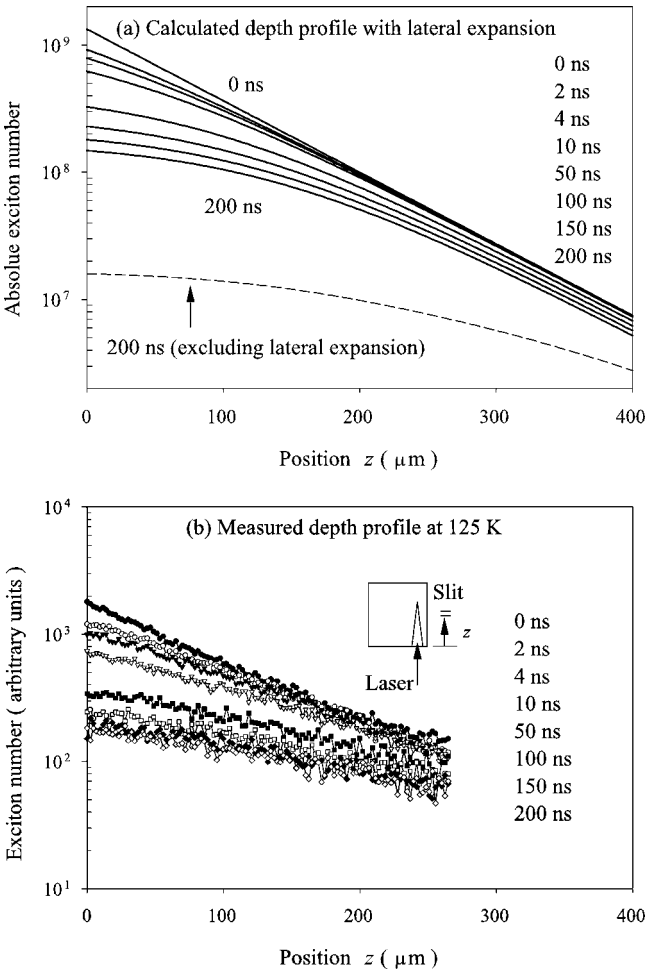

FIG. 15. (a) Simulation of the depth profiles along the laser beam direction (z), taking into account the measured lateral expansion at $T_L=111$ K. The dashed line corresponds to the 200-ns depth distribution excluding the lateral expansion, which affects the capture rate and thus the parametrization of the exciton effective volume. (b) Experimentally measured depth profiles at $T_L=125$ K. The excitation energy is set to 2070 meV corresponding to the absorption length of 100 μm. The inset is a schematic diagram of the depth profile measurement.

$$n(x,y,z,t) = \frac{N(t)}{2\pi\sigma^2(t)d} e^{-(x^2+y^2)/2\sigma^2(t)} e^{-z/d}, \tag{A3}$$

and Eq. (A1) would yield an effective volume given by $V(t)=8\pi\sigma^2(t)d$. However, the density-dependent capture process significantly affects the shape of the depth profile. In order to model the depth profile most simply we assume that a biexciton mostly decays through the Auger process, regenerating one exciton, as in Eq. (12).[41]

Consider first the case in which a reduction in the surface density due to lateral expansion is neglected, i.e., set $\sigma(t)=\sigma(0)$. The depth profile as a function of time becomes

$$N_z(t) = \frac{N_z(0)e^{-t/\tau}}{1+\bar{C}(T)N_z(0)\tau(1-e^{-t/\tau})/4\pi\sigma^2(0)d}, \tag{A4}$$

where the effective volume $V(t)=4\pi\sigma^2(0)d$ is obtained by substituting $N(0)e^{-z/d}[\equiv N_z(0)]$ for $N(0)$. In Fig. 15(a), corre-

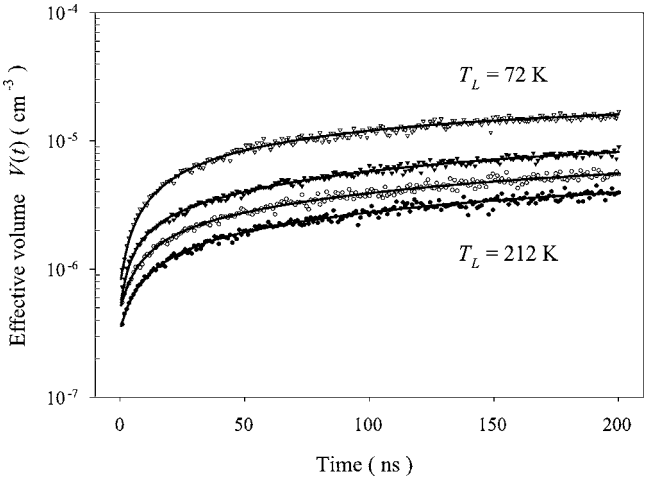

FIG. 16. Effective volume, as defined by Eqs. (A6) and (A7), as a function of time at T_L=72, 111, 162, and 212 K. In each case the experimental inputs are $\sigma(t)$ and $d(t)$. The resulting curves, especially at $t<50$ ns, show that the capture broadening is stronger at lower temperatures.

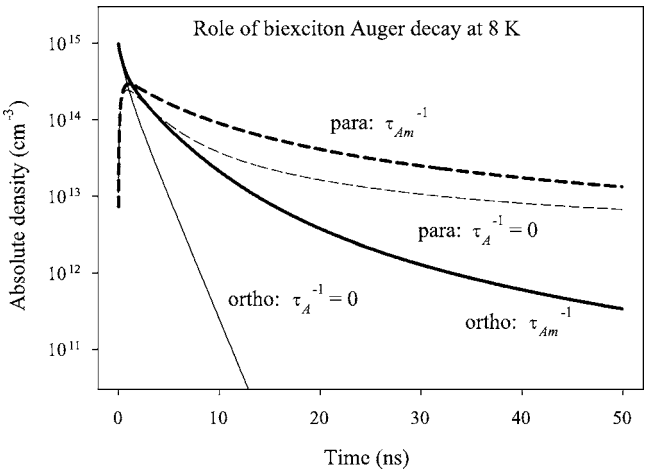

FIG. 17. Impacts on the ortho- and paraexciton densities caused by the biexciton Auger decay for T_L=8 K. The ortho (para) densities are plotted with solid (dashed) curves. For simplicity, we assume $T=T_L$ in the simulations. The heavy curves are generated using our best-fit parameters. The light curves correspond to the *equilibrium* exciton-biexciton population dynamics without Auger decay of biexcitons.

sponding to T_L=111 K, the dashed curve shows a simulation of the exciton depth distribution at t=200 ns due to the capture process, assuming no lateral expansion. The spatial distribution is far from a single exponential because there is stronger exciton capture near the surface. After 200 ns, the calculated decrease in the number of excitons at the surface (z=0), where the exciton loss mechanism is strongest, is almost two orders of magnitude.

In our experiment, however, we must also account for lateral expansion $\sigma(t)$ due to the capture broadening and diffusion. We replace $\sigma(0)$ by the time-dependent $\sigma(t)$ determined by the fits in Fig. 7(b). Now the functional form of the modified depth distribution is given by

$$N_z(t) = \frac{N_z(0)e^{-t/\tau}}{1 + \int_0^t dt' \bar{C}(T) N_z(0) e^{-t'/\tau} / 4\pi\sigma^2(t')d}. \quad \text{(A5)}$$

In Fig. 15(a), solid curves show the calculated depth distributions as a function of time for T_L=111 K. Figure 15(b) is a plot of the observed depth distributions at T_L=125 K where the initial absorption length was set to 100 μm. The simulation qualitatively explains the observed depth profile of Fig. 15(b) quite well.

After considering both lateral and depth distributions, the calculated effective volume $V(t)$ is given by[15]

$$V(t) = 4\pi\sigma^2(t)d \frac{[1+\gamma(t)]\{\ln[1+\gamma(t)]\}^2}{[1+\gamma(t)]\ln[1+\gamma(t)] - \gamma(t)}, \quad \text{(A6)}$$

where $\gamma(t)$ is defined by

$$\gamma(t) = \int_0^t [\bar{C}(T)N(0)/4\pi\sigma^2(t')d] e^{-t'/\tau} dt'. \quad \text{(A7)}$$

In Fig. 16 we plot the effective volume $V(t)$ as a function of time at each temperature. As expected from Fig. 7(b), the effective volume change becomes larger as the temperature decreases, due to the capture broadening. The effective volume given by Eqs. (A6) and (A7) reduces to $V(t) = 8\pi\sigma^2(t)d$ as $\gamma(t)$ approaches 0, corresponding to no density-dependent decay process.

APPENDIX B: AUGER DECAY AND REGENERATION

In Sec. III we discussed the interplay of Auger recombination and the approach to chemical equilibrium. In view of the density-dependent decay rate, it is appropriate to ask how we can distinguish between an Auger process (either exciton or biexciton) and the approach to chemical equilibrium of an exciton-biexciton gas.

An answer to this question lies in the population dynamics of ortho- and paraexcitons. The heavy solid curve in Fig. 17 shows the decay of orthoexcitons at 8 K when the biexciton Auger process is included, as determined by the numerical solution to Eqs. (13). If the biexciton Auger terms are excluded (i.e., $\tau_A^{-1}=0$), the orthoexciton density drops much more rapidly—shown by the light solid curve—because nearly all the orthoexcitons rapidly down-convert to paraexcitons at this temperature. Including the Auger process, on the other hand, regenerates both orthoexcitons and paraexcitons, as seen in the data (e.g., Figs. 12 and 13). The long-lived paraexcitons produce the biexcitons through the capture term $C_p n_p^2$, which in turn causes the long tail in the ortho transient. Ortho regeneration is the signature of an Auger process.

*Present address: Department of Physics and Astronomy, Northwestern University, 2145 Sheridan Road, Evanston, Illinois 60208-3112. Electronic address: joonjang@uiud.edu
†Electronic address: j-wolfe@uiuc.edu

[1] J. P. Wolfe, J. L. Lin, and D. W. Snoke, in *Bose-Einstein Condensation*, edited by A. Griffin, D. W. Snoke, and S. Stringari (Cambridge University Press, Cambridge, England, 1995). Note that the exciton densities in this chapter (and in Refs. 2–5) were extracted from spectroscopic fitting, an assumption that is not supported by absolute measurements of the gas density.
[2] D. Hulin, A. Mysyrowicz, and C. Benoît à la Guillaume, Phys. Rev. Lett. **45**, 1970 (1980).
[3] D. Snoke, J. P. Wolfe, and A. Mysyrowicz, Phys. Rev. Lett. **59**, 827 (1987).
[4] D. W. Snoke and J. P. Wolfe, Phys. Rev. B **42**, 7876 (1990).
[5] J. L. Lin and J. P. Wolfe, Phys. Rev. Lett. **71**, 1222 (1993).
[6] N. Naka, S. Kono, M. Hasuo, and N. Nagasawa, Prog. Cryst. Growth Charact. Mater. **33**, 89 (1996).
[7] M. Y. Shen, T. Yokouchi, S. Koyama, and T. Goto, Phys. Rev. B **56**, 13 066 (1997).
[8] N. Naka and N. Nagasawa, Phys. Status Solidi B **238**, 397 (2003).
[9] K. E. O'Hara, L. Ó Súilleabháin, and J. P. Wolfe, Phys. Rev. B **60**, 10 565 (1999).
[10] K. E. O'Hara, J. R. Gullingsrud, and J. P. Wolfe, Phys. Rev. B **60**, 10 872 (1999).
[11] J. T. Warren, K. E. O'Hara, and J. P. Wolfe, Phys. Rev. B **61**, 8215 (2000).
[12] D. W. Snoke and V. Negoita, Phys. Rev. B **61**, 2904 (2000).
[13] K. E. O'Hara and J. P. Wolfe, Phys. Rev. B **62**, 12909 (2000).
[14] S. Denev and D. W. Snoke, Phys. Rev. B **65**, 085211 (2002).
[15] J. P. Wolfe and J. I. Jang, Solid State Commun. **134**, 143 (2005).
[16] These authors (Kavoulakis and Baym) calculated A_{phonon} in the low-T limit. In Ref. 15 we extended the calculation to nonzero temperatures and found $A_{\text{phonon}}=\text{const}\, D_{12}^2[1+2f(\hbar\omega_{12}/k_BT_L)]$, where D_{12} is the relevant deformation potential and $f(\hbar\omega_{12}/k_BT_L)$ is the occupation number of the optical phonon with energy $\hbar\omega_{12}$. Also we note that $D_{12}=2.5$ eV/Å used by Kavoulakis and Baym to obtain a numerical value for A_{phonon} is much larger than the experimental value 0.12 eV/Å by D. W. Snoke, D. Braun, and M. Cardona, Phys. Rev. B **44**, 2991 (1991), leading to an inflated estimate for A_{phonon}. Our corrected value for A_{phonon} brings its predicted value below that of A_{direct}, which is now predicted to dominate for $T>10$ K (see Ref. 15).
[17] For the phonon-assisted Auger process, the rate starts to increase with temperature at $T>70$ K. Below this temperature, only the spontaneous emission contributes, causing a constant rate.
[18] Preliminary reports of this work are J. I. Jang and J. P. Wolfe, Phys. Rev. B **72**, 241201(R) (2005); and Solid State Commun. **137**, 91 (2006).
[19] The biexciton has possible symmetries $\Gamma_1+\Gamma_3+\Gamma_4+\Gamma_5$ corresponding to para and three ortho states (Ref. 25). The Γ_1 ground state ("para-para") is radiatively forbidden.
[20] Y. Petroff, P. Y. Yu, and Y. R. Shen, Phys. Rev. Lett. **29**, 1558 (1972).
[21] W. F. Brinkman, T. M. Rice, and B. Bell, Phys. Rev. B **8**, 1570 (1973).
[22] W.-T. Huang, Phys. Status Solidi B **60**, 309 (1973).
[23] T. Ohyama, T. Ogawa, and H. Nakata, Phys. Rev. B **56**, 3871 (1997).
[24] C. Klingshirn and H. Haug, Phys. Rep. **70**, 315 (1981).
[25] F. Bassani and M. Rovere, Solid State Commun. **19**, 887 (1976).
[26] Our biexciton formation model mostly depends on the ground state of biexcitons formed by capture of two paraexcitons. In this case, the ground-state degeneracies of excitons and biexcitons are unity.
[27] A. I. Bobrysheva and S. A. Moskalenko, in *Bose-Einstein Condensation*, edited by A. Griffin, D. W. Snoke, and S. Stringari (Cambridge University Press, Cambridge, England, 1995).
[28] The theoretical basis for this assumption is that the phonon-assisted Auger process for the ground state of a biexciton is negligible due to the tiny coupling constant of its constituents, paraexcitons (Γ_2^+), to all optical phonons in this material.
[29] J. I. Jang, Ph.D. thesis, University of Illinois at Urbana-Champaign, 2005.
[30] S. Nikitine, J. B. Grun, and M. Seiskind, J. Phys. Chem. Solids **17**, 292 (1961).
[31] Although ϕ can be eliminated as a fit parameter, it is difficult to determine τ_A from low-T_L data, which can be adequately explained with a capture coefficient alone. However, the fits to the low-T_L data do set a lower limit on τ_A^{-1} that is consistent with the high-T_L determination. For an Auger rate faster than this lowest value, the exciton kinetics is entirely described by $C_p(T)$.
[32] J. I. Jang, K. E. O'Hara, and J. P. Wolfe, Phys. Rev. B **70**, 195205 (2004).
[33] We represent the band-gap shift up to third order as $E_{gap}(T)=E_o-aT^2+bT^3$ where $E_o=2034.13$ meV, $a=0.0017$ meV/K^2, and $b=0.000\,002\,9$ meV/K^3 (solid curve). The result is consistent with the empirical form of $E_{gap}(T)=E_o-\alpha T^2/(1+\beta T)$ proposed by Y. P. Varshi, Physica (Utrecht) **34**, 149 (1967). See also D. W. Snoke, A. J. Shields, and M. Cardona, Phys. Rev. B **45**, 11693 (1992).
[34] Lifetimes in the 300–500-ns range persist to lower temperatures. Measurement of these rates can be affected by the pulse repetition rate, as discussed in Ref. 32.
[35] Our $2\times2\times2.3$-mm sample is cut with all (100) faces.
[36] D. P. Trauernicht and J. P. Wolfe, Phys. Rev. B **33**, 8506 (1986). The temperature dependence of the exciton diffusion constant is proportional to $T_L^{-1/2}$ by acoustic-phonon deformation potential theory.
[37] G. M. Kavoulakis and A. Mysyrowicz, Phys. Rev. B **61**, 16 619 (2000). An experimental attempt to measure the spin-flip rate from the buildup of paraexciton absorption is described in M. Kubouchi, K. Yoshioka, R. Shimano, A. Mysyrowicz, and M. Kuwata-Gonokami, Phys. Rev. Lett. **94**, 016403 (2005); however, their measured orthoexciton loss rate appears to be much slower than the paraexciton buildup rate.
[38] During the mutual spin-flip process an orthobiexciton can decay into two paraexcitons instead of a parabiexciton because it has an exchange energy of 24 meV that is larger than the estimated biexciton binding energy. We find that this modification of the rate equations does not affect our final results.
[39] We use T^{-1}-dependent capture coefficients that change with time. Using Eqs. (13) we also confirm that the T^{-1} dependence persists down to 2 K as described in Ref. 18. In the steady-state method for determining C_p the gas cooling is not a complicating factor.
[40] J. J. Sakurai *Mordern Quantum Mechanics* (Addision-Wesley, Reading, MA, 1985), p. 399.
[41] This approximation is expected to work in the low-temperature

limit where the Auger rate greatly exceeds the dissociation rate. As temperature increases, the Auger rate increases as T but the dissociation rate increases as $T^{1/2}e^{-\phi/k_BT}$, causing both biexciton decay channels to be comparable at $T>30$ K. It is important to note that there is no exciton loss in the dissociation of one biexciton into two excitons. We confirm that any error in the determination of $\bar{C}(T)$ due to this approximation falls into within systematic error bars.